Sensitivity of Australian Rainfall to Inter–El Niño Variations

GUOMIN WANG AND HARRY H. HENDON

Bureau of Meteorology Research Centre, Melbourne, Australia

(Manuscript received 12 June 2006, in final form 5 December 2006)

ABSTRACT

Australia typically experiences drought during El Niño, especially across the eastern two-thirds of the continent during austral spring (September–November). There have, however, been some interesting departures from this paradigm. For instance, the near-record-strength El Niño of 1997 was associated with near-normal rainfall. In contrast, eastern Australia experienced near-record drought during the modest El Niño of 2002. This stark contrast raises the issue of how the magnitude of the drought is related to the character and magnitude of El Niño, for instance as measured by the broadscale sea surface temperature (SST) anomaly in the equatorial eastern Pacific. Internal (unpredictable) atmospheric noise is one plausible explanation for this contrasting behavior during these El Niño events. Here, the authors suggest that Australian rainfall is sensitive to the zonal distribution of SST anomalies during El Niño and, in particular, the greatest sensitivity is to the SST variations on the eastern edge of the Pacific warm pool rather than in the eastern Pacific where El Niño variations are typically largest. Positive SST anomalies maximized near the date line in 2002, but in 1997 maximum anomalies were shifted well into the eastern Pacific, where their influence on Australian rainfall appears to be less. These findings provide a plausible physical basis for the view that forecasting the strength of El Niño is not sufficient to accurately predict rainfall variations across Australia during El Niño.

1. Introduction

Australia typically experiences drought during El Niño when the Southern Oscillation swings into its negative phase, especially across the eastern two-thirds of the continent in austral spring (McBride and Nicholls 1983; Ropelewski and Halpert 1987; Allan 1988). Similarly, Australia typically receives above-normal rainfall during La Niña when the Southern Oscillation swings into its positive phase. The strength of this relationship and the tendency for El Niño/La Niña conditions to persist once established in austral winter (June–August) can be exploited to make skillful rainfall forecasts one or more seasons in advance (e.g., Drosdowsky and Chambers 2001). However, two recent El Niños (1997 and 2002; Fig. 1) raise the interesting issue of whether the magnitude of El Niño–induced drought is linearly related to the magnitude of El Niño, for instance as measured by indices of sea surface temperature (SST) in the equatorial eastern equatorial Pacific. The near-record-strength El Niño of 1997 was associated with near-normal to above-normal rainfall across most of the country during spring (September–November; Fig. 1a). The seasonal forecasts for springtime rainfall in 1997 from various forecast centers, which called for drought conditions, were failures and resulted in a setback in public confidence of seasonal climate forecasts (e.g., Goddard et al. 1998, 2001). In contrast, during the modest El Niño of 2002 eastern Australia experienced near-record drought (Fig. 1b), resulting in significant economic disruption as reflected in a ~25% drop of Australia's gross farm product (Lu and Hedley 2004).

Obviously there is a need to understand the cause of these unexpected rainfall anomalies during these contrasting El Niños in light of the long-term statistical relationship between El Niño and Australian rainfall that is exploited to make seasonal prediction. Power et al. (2006) recently studied the relationship between common indices of the state of the El Niño–Southern Oscillation (ENSO) and observed and simulated Australian-mean rainfall. They found that annual-mean Australian rainfall tends to linearly increase with the strength of La Niña, whereas the decline with El Niño is much less linear. In other words, while the strength of La Niña is a good indication of the magnitude of the

Corresponding author address: G. Wang, Bureau of Meteorology Research Centre, GPO Box 1289, Melbourne 3001, Australia. E-mail: g.wang@bom.gov.au

DOI: 10.1175/JCLI4228.1

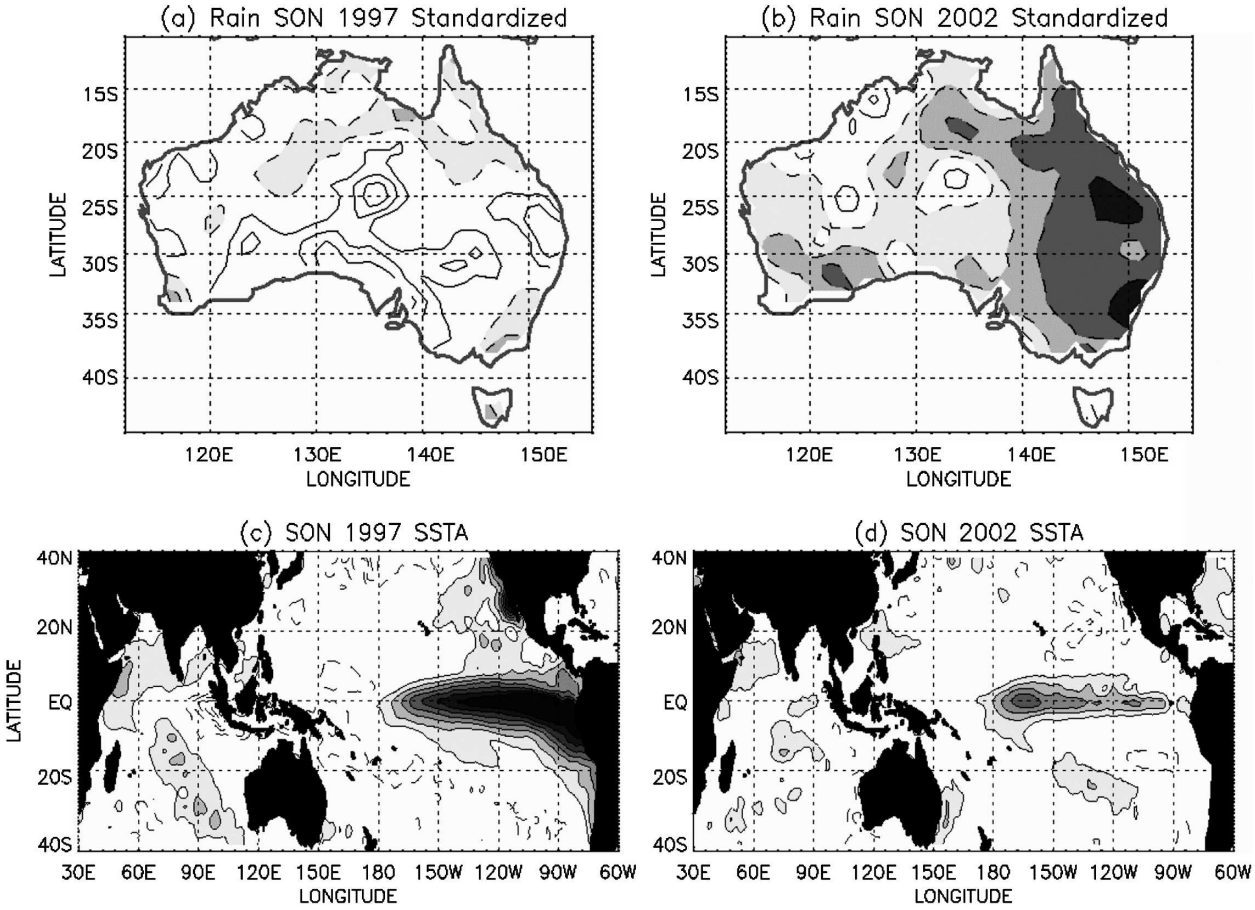

FIG. 1. (a),(b) Australia rainfall and (c),(d) Indo-Pacific SST anomalies during SON (a),(c) 1997 and (b),(d) 2002. Rainfall anomalies have been standardized and contours are drawn from ±0.4 with an interval of 0.4. SST anomalies are drawn from ±0.5°C with an interval of 0.5°C. Positive and negative contours are drawn with solid and dashed lines, respectively. Negative rainfall and positive SST anomalies are also highlighted with progressive shadings. Spatial smoothing has been applied for rainfall anomalies before drawing.

associated positive rainfall anomaly, the strength of El Niño is not a good indication of the magnitude of the associated rainfall reduction. Power et al. (2006) restricted their attention to annual mean Australian rainfall and its relationship to traditional measures of the state of ENSO (e.g., the Southern Oscillation index) and did not investigate the cause of the lack of linear relationship with El Niño.

Internal (unpredictable) atmospheric noise is one plausible explanation for the contrasting behavior of 1997 and 2002. Here, we explore the possibility that the differing structure of tropical SST anomalies in these two El Niños is at the root of the discrepancy. SST anomalies in the equatorial Pacific in late 1997 exhibited "typical" characteristics of mature El Niño (e.g., Rasmusson and Carpenter 1982), with the strongest positive SST anomalies developing in the far eastern Pacific (Fig. 1c). Here we define the typical El Niño as having spatial distribution of SST anomaly similar to that revealed, for example, by the leading empirical orthogonal function of SST (e.g., as shown in Fig. 7a). In contrast, positive SST anomalies at the peak of the 2002 event were essentially confined to the central Pacific, with only weak warm anomalies evident in the eastern Pacific (Fig. 1d). Importantly, the central Pacific SST anomalies were stronger in 2002 than in 1997, even though the anomalies were smaller than those that typically develop in the eastern Pacific during El Niño. The anomalies just east of the date line are important to the atmospheric response during El Niño because they occur in a region of higher mean SST than farther east, hence they are efficient at driving anomalous convection and remote circulation changes (Graham and Barnett 1987; Sardeshmukh and Hoskins 1988; Hoerling and Kumar 2002). Furthermore, the 2002 El Niño event was associated with only small SST anomalies in the far

western Pacific and Indian Ocean, while the 1997 event exhibited significant negative SST anomalies in these regions.

The hypothesis that we will thus explore is that Australian rainfall is sensitive to the detailed distribution of tropical SST anomalies during El Niño and, importantly, is most sensitive to the variations of SST in the central and western Pacific where SST is climatologically highest. This hypothesis is supported by the recent results of Potgieter et al. (2005), who implicated central Pacific SST variations as important drivers of eastern Australian rainfall and wheat yield.

A similar hypothesis has been explored to account for the inter–El Niño variability of the teleconnection into the North Pacific–American sector (e.g., Kumar and Hoerling 1997; Hoerling and Kumar 2002). These studies conclude, however, that the tropically forced, extratropical circulation anomaly in the North Pacific–American sector consists largely of a single spatial structure, whose strength increases linearly with the strength of El Niño as monitored, for instance by, the Niño-3 SST index (SST averaged over 5°S–5°N, 90°–150°W). Any variations in the extratropical response as a result of inter–El Nino variations in the pattern of tropical SST anomaly are swamped by internal atmospheric variability and by sensitivity to spatial variations of the mean state through which the response propagates (e.g., Trenberth et al. 1998).

This conclusion might not necessarily apply to Australia because El Niño–induced climate variations here are a more direct response to anomalous tropical convection driven by equatorial Pacific SST anomalies. For instance, Australia directly experiences the western pole of the Southern Oscillation with surface pressure increased across much of tropical and eastern Australia during El Niño. In contrast, the effects of El Niño are communicated into the Northern Hemisphere extratropics via excitation of Rossby waves that propagate through a wavy basic state (e.g., Sardeshmukh and Hoskins 1988; Trenberth et al. 1998).

In the present study, we will explore the sensitivity of Australian rainfall to inter–El Nino variations of tropical SSTs based on observations for two recent decades (1982–2002), for which SST and atmospheric analyses are most reliable. We will demonstrate maximum sensitivity of Australian rainfall to the SST anomalies during El Niño in the central equatorial Pacific, especially just east of the date line. This sensitivity is confirmed by projection of independent data from two earlier decades (1961–81) onto the patterns of variability revealed in the recent record. These results suggest that simply forecasting the magnitude of an El Niño event without regard to the spatial structure of the SST anomalies will not be sufficient to adequately predict the associated rainfall anomalies in Australia. However, it remains unclear whether the relevant details of the inter–El Niño SST variations are themselves predictable. We will return to this issue in section 5.

2. El Niño 1997 versus 2002

We begin by examining in more detail the differences in the anomalies of SST, convection, and circulation during the El Niño events of 1997 and 2002. We will focus on austral spring [September–November (SON)] season, when El Niño's influence on Australian rainfall is the strongest (e.g., McBride and Nicholls 1983). The preliminary inspection of the SST anomalies, derived from the dataset of Reynolds and Smith (1994), revealed that the warmest anomaly was centered eastward of 150°W in 1997 but farther to the west in 2002 (Figs. 1c,d). Inspection of the actual (i.e., anomaly plus climatology) SST along the equator (Figs. 2a,b) reveals that the SST was higher just east of the date line in 2002 (exceeding 30°C near 165°W) than in 1997 (~29°C). However, SST exceeded the threshold for deep convection (~27.5°C) all the way across the east Pacific in 1997 but was limited to west of about 150°W in 2002. Furthermore, only small SST anomalies were evident in the western Pacific (130°E–180°) and Indian Ocean in 2002, while in 1997 SST was slightly below normal in the western Pacific and sharply below normal in the eastern Indian Ocean (80°–100°E).

The corresponding distribution of atmospheric deep convection is inferred from outgoing longwave radiation (OLR; Figs. 2c,d), which we obtain from the dataset described by Liebmann and Smith (1996). Anomalously low OLR (enhanced convection) occupies the entire eastern Pacific in 1997, consistent with the SST there being everywhere above 27.5°C. In 2002 enhanced convection is limited to west of 150°W. Furthermore, convection in the central-western Pacific was more intense in 2002 than in 1997 (i.e., minimum OLR is about 210 W m^{-2} near 165°E in 2002 while the minimum in 1997 was about 220 W m^{-2} centered near 165°W), consistent with the occurrence of warmer SST in the central and western Pacific in 2002. Farther west, convection was slightly suppressed (i.e., OLR was above normal) over the Maritime Continent (100°–145°E) but near normal over much of the Indian Ocean in 2002, where SST was near normal. On the other hand, convection was significantly suppressed (larger positive OLR anomalies) over the Maritime Continent and eastern Indian Ocean in 1997, coincident with the occurrence of negative SST anomalies there. And, far-

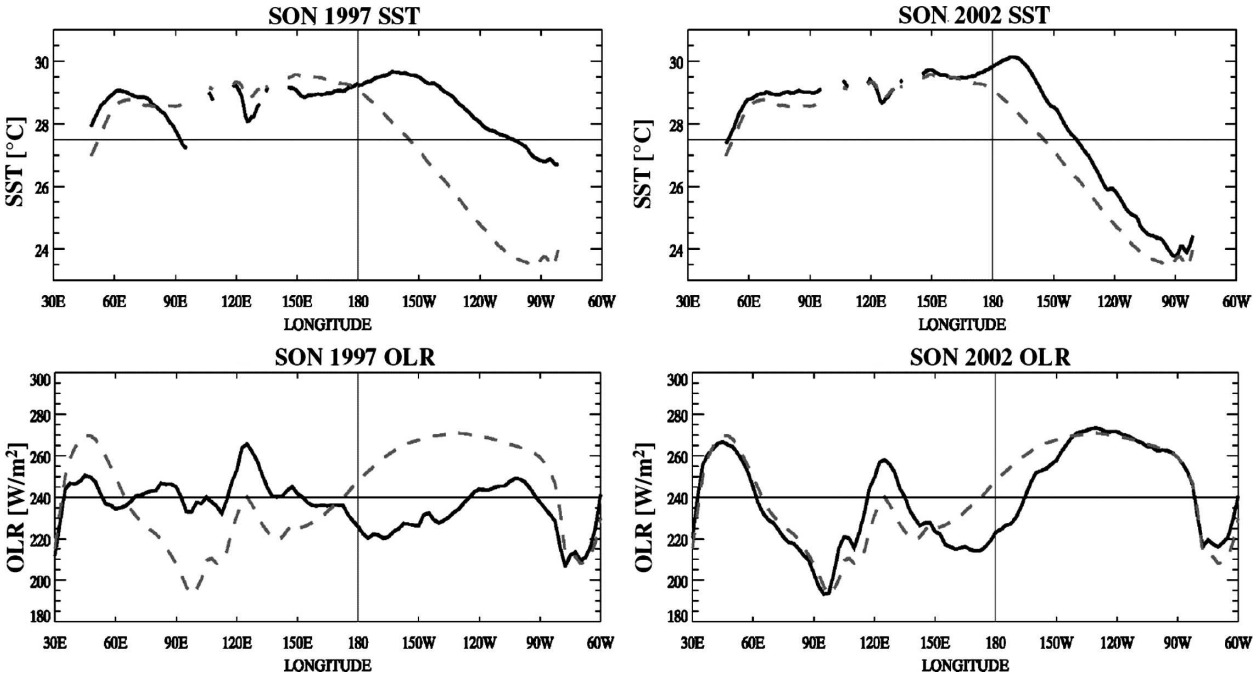

FIG. 2. SST and OLR vs longitude. Solid curves are (top) SST and (bottom) OLR averaged between 5°N and 5°S for SON (left) 1997 and (right) 2002. Dashed curves are the respective climatological distributions.

ther west over eastern Africa (30°–45°E), convection was enhanced in 1997 but near normal in 2002.

The above analysis implies substantial differences in the Walker circulation between 1997 and 2002. The anomalous Walker circulation is depicted in Fig. 3 by vectors whose horizontal components are the divergent zonal wind anomalies and whose vertical components are the pressure vertical velocities anomalies (note that the plotting convention is that upward pointing implies upward motion). The wind anomalies were derived from the National Centers for Environmental Prediction–Department of Energy (NCEP–DOE) Reanalysis 2 dataset (Kanamitsu et al. 2002).

The anomalous ascending branch in the eastern Pacific is centered on 135°W in 1997 (Fig. 3a), while in 2002 it is centered farther west at about the date line (Fig. 3b). Furthermore, the anomalous ascending branch covers the entire eastern Pacific in 1997, while in 2002 it is confined within about 15° longitudes of the date line. In 1997 the entire western Pacific and eastern Indian Ocean experiences anomalous descent, but with strongest descent centered just east of Australia at about 150°E. Another upward branch is also evident farther west over eastern Africa, consistent with enhanced convection as implied by negative OLR anomalies there. In contrast, the descending branch is narrower in 2002 and is centered more over the Maritime Continent (i.e., at Australian longitudes), and there is little evidence of an anomalous upward branch farther west in the Indian Ocean.

The spatial distribution of upper-level divergence and convergence is depicted by maps of anomalous velocity potential and divergent wind at 200 hPa (Fig. 4). Maximum divergence (outflow) in the eastern Pacific is stronger in 1997, but its center is located well east of that in 2002. Similarly, the strongest convergence over the west Pacific is shifted eastward in 1997 compared to 2002. Focusing on the Australian region, a convergence line is situated over the southwest Pacific Ocean just off the northeast coast of Australia in 1997. In contrast, the dominant convergence line in 2002 is located inland over northeast Australia.

The streamfunction and rotational wind anomalies are shown in Fig. 5. In both years there is an upper-level anticyclonic pair over the central Pacific, which is well understood as the response to enhanced diabatic (convective) heating (e.g., Gill 1980). The pair is less easterward extended and the easterly anomaly in between the pair is weaker in 2002 and located west of its counterpart in 1997. Farther west over the Indian Ocean, a strong cyclonic pair is evident in 1997, which is also well understood as the response to suppressed diabatic heating (suppressed convection as implied by enhanced OLR) that occurred in the Indian Ocean region in 1997

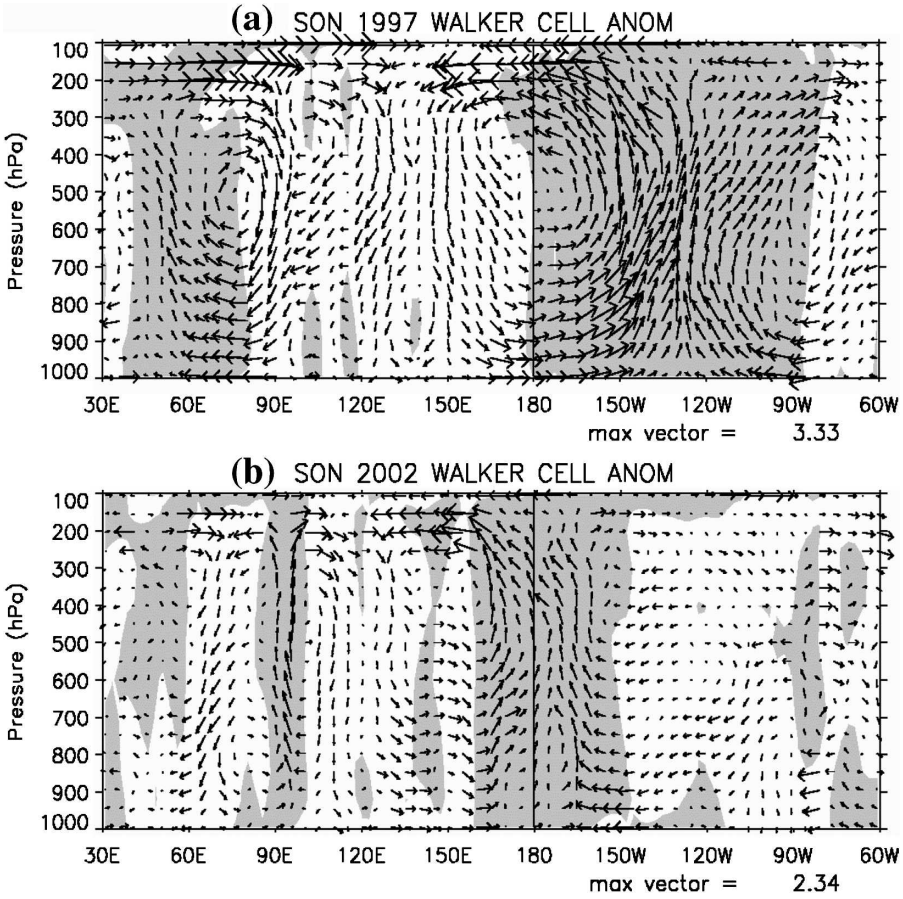

FIG. 3. Anomalous Walker circulation during SON (a) 1997 and (b) 2002 depicted by vectors consisting of the divergent zonal wind anomaly (horizontal component; units: m s^{-1}) and pressure vertical velocity anomaly (vertical component scaled by -2×10^{-2} Pa s^{-1}) averaged over 5°S–5°N. Ascending regions are shaded. Maximum vector magnitude (m s^{-1}) is displayed in lower right of each panel.

(cf. Fig. 2). Only weak evidence of this cyclonic pair is seen in 2002. In the Australian region, weak anticyclonic flow is evident over eastern Australia in 2002, whereas during 1997 most of the continent experiences pronounced cyclonic flow at 200 hPa.

In summary, maximum positive SST anomalies were spread well into the eastern Pacific during the El Niño of 1997, while during the El Niño of 2002 positive SST anomalies were confined to the vicinity of the date line. The accompanying convection and circulation anomalies showed a similar eastward displacement in 1997 compared to 2002, which appears to have resulted in less sinking motion over Australia in 1997 as compared to 2002. The implication, which we will explore below, is that Australian rainfall is more sensitive to SST anomalies at the eastern edge of the Pacific warm pool than it is to the larger anomalies that typically develop farther east in the Pacific during El Niño.

3. Australian rainfall and central Pacific SST during 1982–2002

a. Australian-mean rainfall

The sensitivity of Australian rainfall to central Pacific SST is explored using data for the period 1982–2002. To emphasize the association of drought with the occurrence of El Niño, we form an Australian Drought Index (ADI), which is simply the negative of the Australian-mean rainfall anomaly: positive ADI implies drought. The ADI is derived from the analyses created by the Australian Bureau of Meteorology National Climate Centre (Jones and Weymouth 1997). This analysis uses a successive correction scheme to produce a monthly analysis on a ¼° grid using all available high-quality gauge data. A reduced resolution subset (at 1° spatial resolution) has been used in this study.

The correlation between Indo-Pacific SSTs (Reyn-

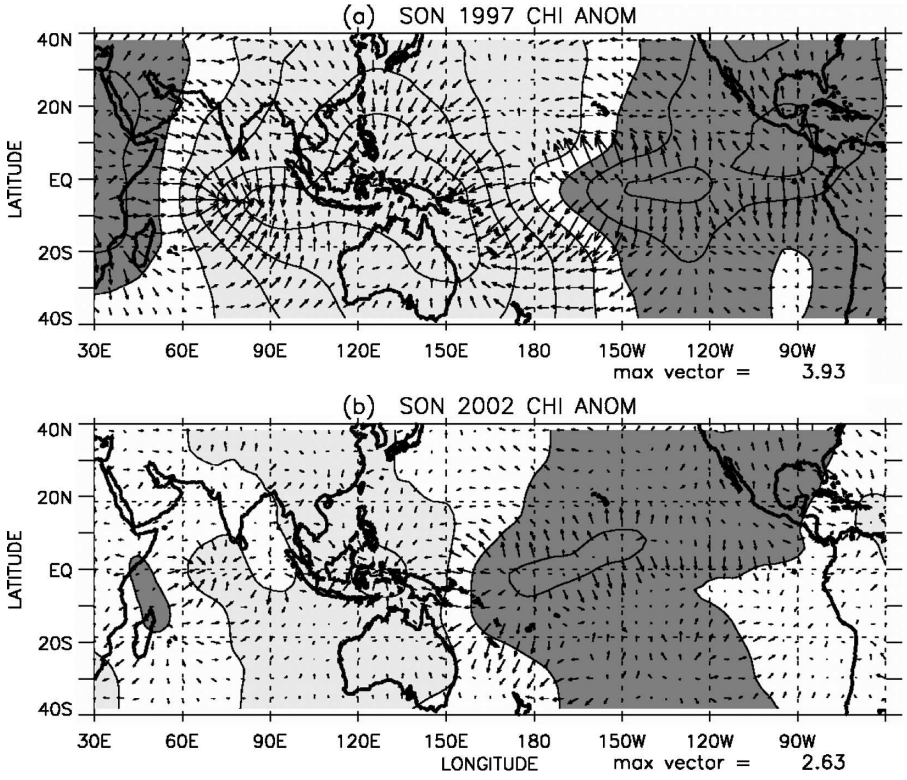

FIG. 4. Anomalous divergent winds (vectors) and velocity potential (contour with shading) at 200 hPa during SON (a) 1997 and (b) 2002. Contour interval for velocity potential is 20×10^5 $m^2\ s^{-1}$ starting from $\pm 10 \times 10^5$ $m^2\ s^{-1}$, and positives and negatives are highlighted with light and dark shading, respectively. Vector wind maximum ($m\ s^{-1}$) is displayed in lower right of each panel.

olds and Smith 1994) and the ADI for SON is shown in Fig. 6a. Drought conditions are associated with warm SST anomalies in a widespread region in the central equatorial Pacific but with the maximum correlation exceeding 0.6 occurring just east of the date line. Also, drought is accompanied by below-normal SST surrounding Australia. Drought conditions are also associated with a southwest–northeast-oriented SST dipole in the southern Indian Ocean. All of these features have been previously associated with Australian rainfall variability (e.g., Nicholls 1989; Drosdowsky and Chambers 2001). The overall pattern of SST correlation associated with drought is broadly typical of that during El Niño, except the correlation is small in the eastern Pacific where SST anomalies are typically maximum during El Niño. The maximum correlation in the central Pacific reinforces the notion that SST anomalies there are the most important drivers of Australian rainfall variability.

The upper-tropospheric circulation anomalies that accompany drought are depicted by regression of 200-hPa velocity potential and divergent wind (Fig. 6b) and streamfunction and rotational wind (Fig. 6c) onto ADI. Anomalies are scaled for a one standard deviation anomaly of ADI and vectors are plotted in black where the associated regression coefficients are judged to be significantly different from zero at the 90% level.

Consistent with conditions during 2002, the Walker circulation is displaced to just east of the date line during drought (Fig. 6b). Convergence in the upper troposphere extends southward across Australia, consistent with the notion that reduced rainfall is associated with anomalous sinking motion. The region of outflow near the date line corresponds with the region of most positive SST correlation and is consistent with this being the region of enhanced convection forced by high SST. Similarly, the streamfunction and rotational wind anomalies associated with Australian drought (Fig. 6c) are consistent with the steady response (e.g., Gill 1980) to regions of enhanced tropical convection near the date line and suppressed convection over the Maritime Continent. Anticyclones centered near the date line straddle the region of warm SST and enhanced convection and a cyclone is evident to the south of the region

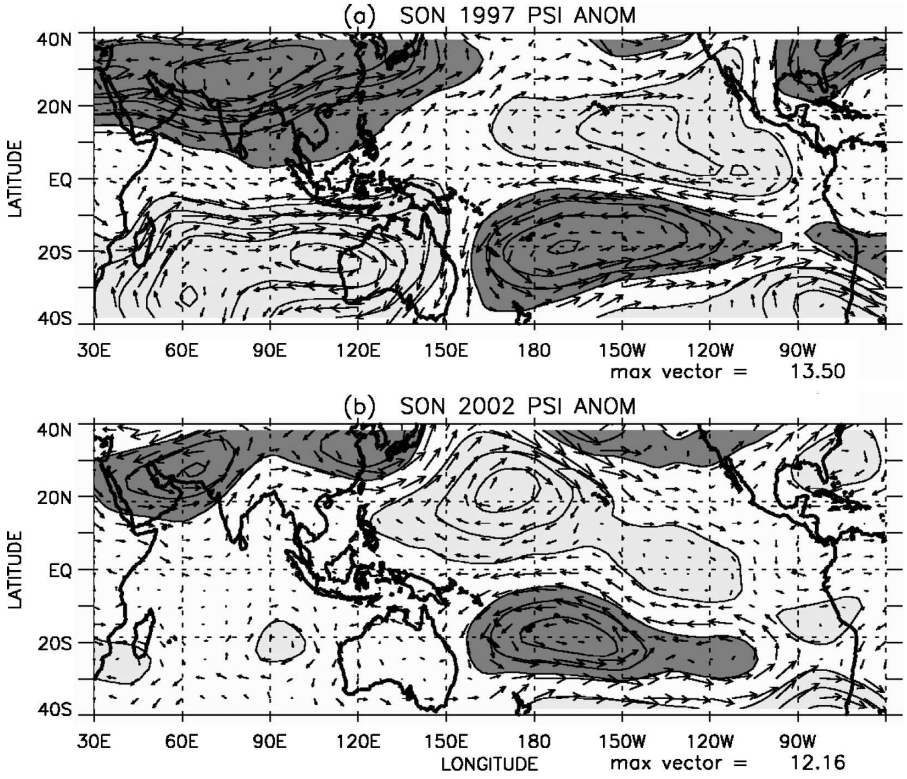

FIG. 5. Anomalous rotational winds (vectors) and streamfunction (contour with shading) at 200 hPa during SON (a) 1997 and (b) 2002. Contour interval for streamfucntion is 30×10^5 m^2 s^{-1} starting from $\pm 30 \times 10^5$ m^2 s^{-1}, and positives and negatives are highlighted with light and dark shading, respectively. Vector wind maximum (m s^{-1}) is displayed in lower right of each panel.

of suppressed convection in the Maritime Continent. During drought most of Australia is under the influence of northerly anticyclonic flow.

An alternative way of emphasizing the importance of equatorial SST/convection anomalies in the central Pacific for driving Australian rainfall variability is to correlate ADI with various indices of El Niño. The correlations with the Niño-4 (5°S–5°N, 160°E–150°W), Niño-3.4 (5°S–5°N, 170°–120°W), and Niño-3 SST indices, which reflect SST conditions in the equatorial central, central-east, and east Pacific, respectively, are 0.58, 0.53, and 0.44, respectively. Consistent with our hypothesis, correlation with ADI monotonically decreases as the SST index region is moved eastward.

b. Sensitivity of rainfall to leading modes of SST variability

This sensitivity of Australian rainfall to Indo-Pacific SST anomalies is further explored by assessing the relationship of Australian rainfall with the leading patterns of SST variability. These are identified by empirical orthogonal function (EOF) analysis based on the SST covariance matrix for the domain 40°S to 30°N and 30°E to 70°W. The associated Australian rainfall variations are obtained by regression (and correlation) onto the principal component (PC) time series of the leading EOFs of SST. We limit our analysis to the first three EOFs of SST. This is somewhat a subjective choice, but these three modes account for about ~70% of the Indo-Pacific SST variance and ~50% of the covariance with Australian-mean rainfall.

The three leading EOFs of SST and their PCs are shown in Fig. 7. The first mode (hereafter SST1) accounts for 51% of the SON SST variance and has structure associated with mature El Niño conditions: positive SST anomaly occupies the majority of the equatorial east Pacific, surrounded by a boomerang-shaped cold anomaly to the west that extends into the eastern equatorial Indian Ocean (Fig. 7a). Its PC time series correlates strongly with traditional indices of ENSO (e.g., correlation with Niño-3 SST index >0.9) and displays large loadings in 1982 and 1997 (two strong El Niño events; see Fig. 7d) and large negative loading in 1988 (strong La Niña event).

The second mode (hereafter SST2) accounts for 12% of the SST variance and exhibits a zonal dipole struc-

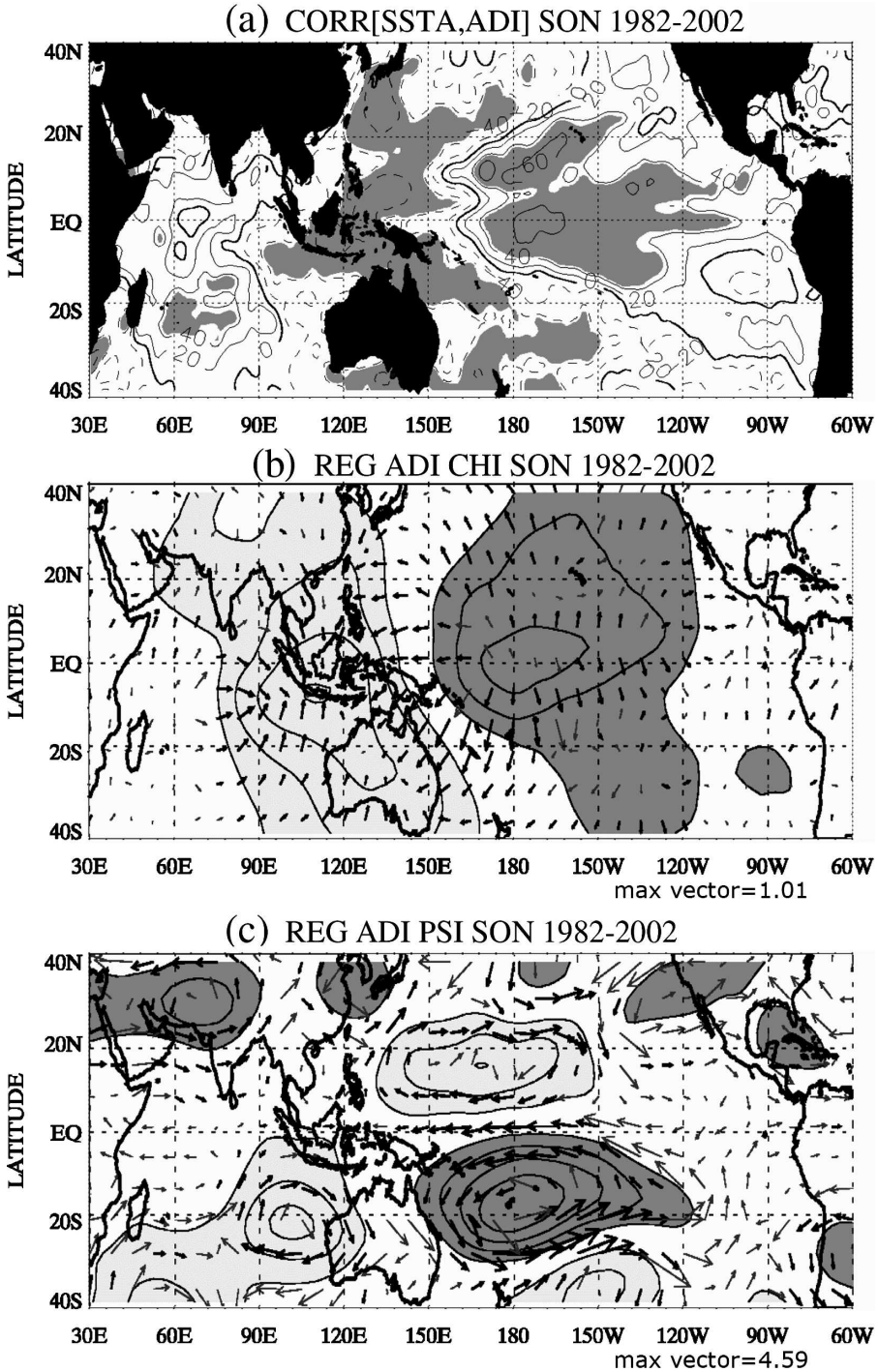

FIG. 6. (a) Correlation of SST with ADI, and regression of (b) 200-hPa divergent wind (vectors) and velocity potential (contour with shading) anomalies and (c) 200-hPa rotational wind (vectors) and streamfunction (contour with shading) anomalies onto ADI. Contour interval in (a) is 0.2, (b) 5×10^5 m^2 s^{-1} from $\pm 5 \times 10^5$ m^2 s^{-1}, and 10×10^5 m^2 s^{-1} from $\pm 10 \times 10^5$ m^2 s^{-1}. The shaded area in (a) indicates that correlation is significant at the 90% level. Vectors in (b) and (c) are bold black where the regression coefficient of either zonal or meridional wind components is significant at the 90% level. Maximum wind vector (m s^{-1}) is indicated in lower right of each panel.

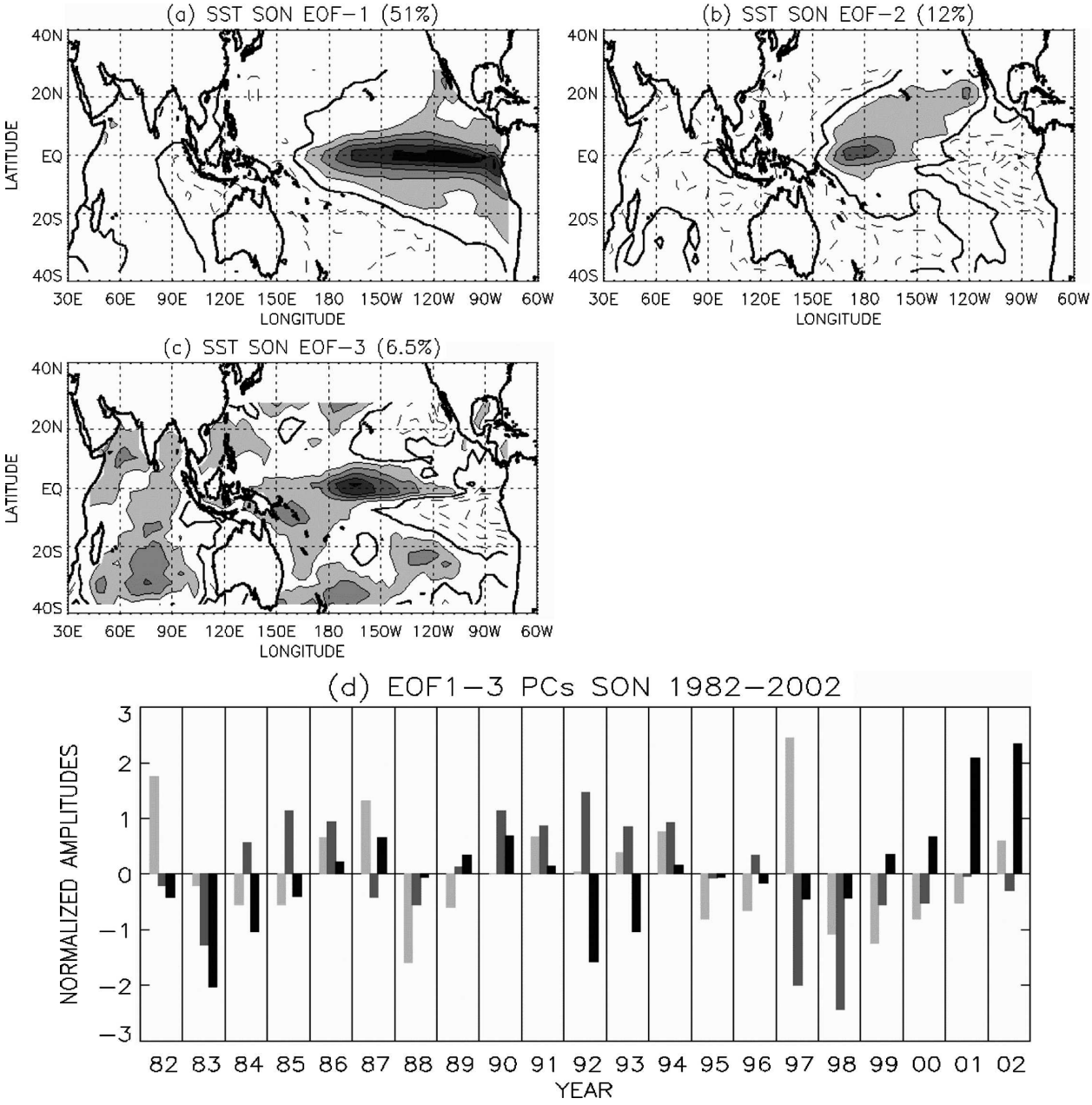

FIG. 7. (a)–(c) First three EOFs of SST derived from dataset covering SON 1982–2002. Positive and negative contours are drawn by thin solid and dashed lines, respectively, with a contour interval of one arbitrary unit. The zero contour is indicated by a heavy solid line and positive contours above 1 are highlighted by progressive shadings. (d) The corresponding principal component time series displayed in histogram format with first, second, and third modes in light, moderate, and dark shading, respectively.

ture in the equatorial Pacific with two oppositely signed anomalies, one in the far east and the other centered on the date line (Fig. 7b). Weaker anomalies surround Australia. This mode projects strongly onto the Trans-Niño Index of Trenberth and Stepaniak (2001) and has been associated with the evolution of ENSO that has occurred post-mid-1970 whereby warm anomalies near the date line precede general warming of the eastern Pacific by a few months. However, the analysis here is based on only the SON season, so SST2 is viewed as a component of inter–El Niño variability. SST2 displays large negative loading in the 1997 El Niño event, consistent with occurrence of maximum SST anomaly in the far eastern Pacific for this event (e.g., Fig. 1c). On the other hand, SST2 displays weak loading in the 1982 event.

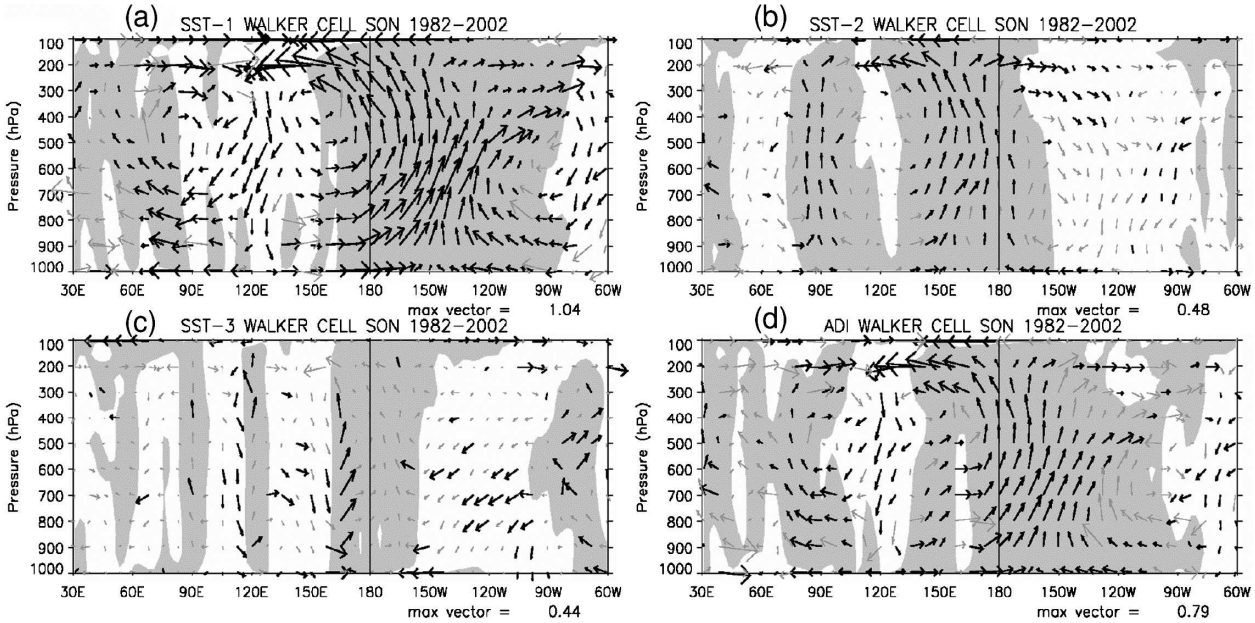

FIG. 8. Regressions of anomalous Walker circulation onto (a) SST1, (b) SST2, and (c) SST3 and onto (d) ADI. Plotting convention is as in Fig. 3. Vectors whose components are significant at the 90% level are drawn in bold black.

The third mode (hereafter SST3) accounts for only 6.5% of the variance. However, the large loading in the central Pacific (Fig. 7c) suggests a possible important role for Australian rainfall. It displays small negative loading in the 1982 and 1997 El Niño events, but strong positive loading in the weak 2002 El Niño, when SST anomalies were a maximum in the central Pacific (e.g., Fig. 1d).

Anomalies in the Walker circulation that are associated with these EOFs of SST are depicted by regression of the divergent zonal wind and pressure vertical velocity onto the respective PCs (Fig. 8). The anomalies, plotted as vectors, are scaled for a one-standard-deviation anomaly of the respective PCs. The anomalous Walker circulation associated with SST1 (Fig. 8a) is characterized by an eastward shift of the upward branch into the eastern Pacific to about 135°W. The downward branch is centered over the Maritime Continent, with another upward branch in the western Indian Ocean. These features are typical of El Niño and are indicative of enhanced convection in the eastern Pacific and suppressed convection over the Maritime Continent.

The Walker circulation anomaly associated with SST2 (Fig. 8b) exhibits a dominant ascending branch just west of the date line, with weaker descent in the far eastern Pacific and in the Indian Ocean. This pattern of ascent and descent is consistent with the longitudinal distribution of SST anomalies associated with SST2. By inference, El Niño events (positive loading on SST1) that are accompanied by a negative projection onto SST2 will have reduced ascent in the vicinity of the date line and enhanced ascent in the eastern Pacific. At the same time, descent would be strengthened and broadened in the Indian Ocean.

The Walker circulation anomaly associated with SST3 is weaker than for SST1 and SST2 (Fig. 8c) but exhibits narrow ascent near the date line and descent in the eastern Pacific. Again, this anomalous pattern of ascent/descent along the equator is consistent with the zonal dipole structure of SST anomalies associated with SST3 (Fig. 7c).

For comparison, the Walker circulation anomalies associated with Australian drought are depicted by regression of the divergent zonal wind/pressure vertical velocity onto ADI (Fig. 8d). The resulting pattern can be interpreted as the "optimal" Walker circulation configuration associated with Australia-wide drought. Overall it looks broadly similar to the response to SST1 (Fig. 8a), but scrutiny reveals that the ascending branch in the central Pacific is shifted westward by ~20° longitude, and descent over the Maritime Continent is less pronounced. Thus, the optimal pattern for drought appears to be a combination of the response associated with positive SST1, supplemented by the westward shift due to SST2 and SST3 (quantified below).

The sensitivity of Australian-mean rainfall to the zonal displacement of the Walker circulation is further quantified by correlation of ADI with the leading PCs of SST (Table 1). As expected, SST1 is positively cor-

TABLE 1. Correlation (in percentage) between ADI and first three PCs of SST EOF over Indo-Pacific Oceans. Boldface (italics) indicates correlations are significant at the 95% (90%) level. Percentage variances explained by each component are also given in the second row.

ADI	PC1	PC2	PC3	Sum
Correlation (%)	**53**	*40*	22	—
Variance (%)	28	16	5	49

related (0.53; significant at the 95% level assuming 20 independent samples) with ADI, reconfirming the notion that drought accompanies mature El Niño. SST2, though explaining much less SST variance, has a similar positive correlation with rainfall (0.4; significant at the 90% level). Negative projection onto SST2 (i.e., cold anomalies in the vicinity of the date line together with warm anomalies in the east Pacific) in conjunction with large projection onto SST1 would mitigate dry conditions associated with typical El Niños, as may have occurred in 1997. The correlation of SST3 with ADI is weakly positive (0.22), but as will be shown below, SST3 plays an important role in explaining regional rainfall variations primarily in the southeast, especially in particular years (e.g., 2002).

Thus, drought is associated with an SST pattern (Fig. 6a) that is a combination of the typical El Niño pattern (SST1) together with contributions from SST2 and SST3 that act to weaken the contribution of eastern Pacific SST and enhance the contribution of central Pacific SST. Together, this optimal combination of SST patterns acts to promote an anomalous Walker circulation that is shifted to the west of its location during a typical El Niño.

The relationship of regional rainfall with the leading EOFs of SST is depicted by regression of gridded rain-

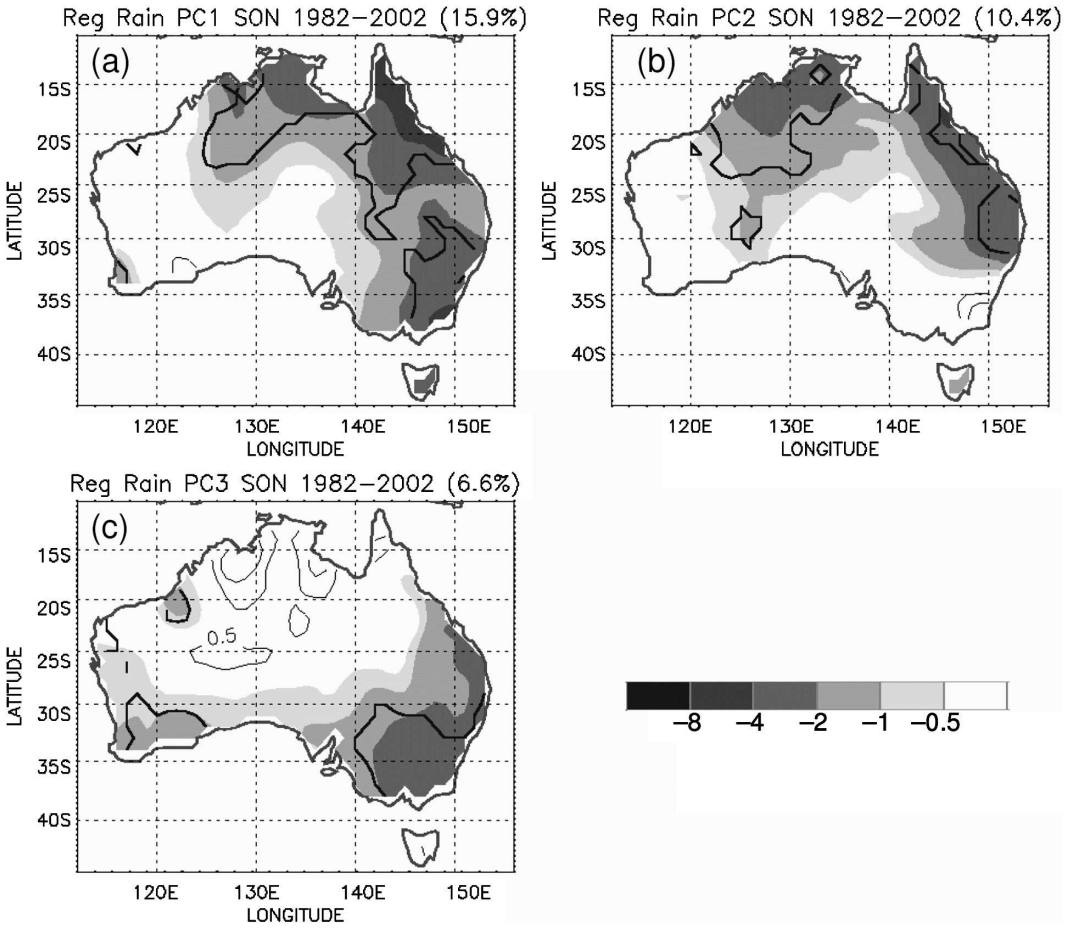

FIG. 9. Regression of Australian rainfall onto (a) SST1, (b) SST2, and (c) SST3. The rainfall variance across the entire continent explained by each SST mode is displayed in upper right of each panel. Positive and negative regressions are drawn by thin solid lines and progressive shadings, respectively, and at levels of ±0.5, 1, 2, 4, and 8×10^{-1} mm day^{-1}. Regressions in areas encompassed by thick solid curves are significant at the 90% level.

fall onto the PCs of the three leading EOFs of SST (Fig. 9). The patterns are scaled for a one-standard-deviation anomaly of the respective PCs. Also indicated above each panel is the total rainfall variance across Australia that is explained by the linear relationship with each PC. These explained variances are about one-half that for Australian-mean rainfall (Table 1) due to spatial incoherence of the gridded rainfall. The rainfall pattern associated with SST1 shows the drought pattern over eastern and northern Australia that typifies El Niño (e.g., Ropelewski and Halpert 1987). The pattern associated with SST2 is similar in strength and structure to that of SST1 except it is weak in the southeast corner. The pattern associated with SST3 is again broadscale but mainly concentrated in the southeast, where it locally accounts for as much variance as does SST1.

The above analyses indicate that sensitivity of Australian rainfall extends beyond that associated with the typical distribution of SST during El Niño. Although the leading mode of SST variability (SST1) accounts for more than 50% of the Indo-Pacific SST variance, Australian rainfall is nearly as sensitive to SST2, but only accounts for just over 10% of the SST variance. A similar picture emerges for SST3.

We propose that this sensitivity to SST on the eastern edge of the warm pool, as indicated by the strong sensitivity of Australian rainfall to the SST EOFs 2 and 3, occurs because small SST anomalies on the eastern edge of the warm pool here drive large changes in convection (e.g., Hoerling and Kumar 2002). Furthermore, SST anomalies on the eastern edge of the warm pool are in closer proximity to Australia so that they drive perturbations to the Walker circulation that more directly affect Australian rainfall.

c. Reassessment of 1997 and 2002

The difference in rainfall anomalies during the 1997 and 2002 El Niños can now be reassessed by reconstructing the rainfall anomalies based on regression onto the leading EOFs of SST. Because of the orthogonality of the PCs, the individual regression patterns are multiplied by the respective PC values each year, and then simply summed over the three leading EOFs (Fig. 10). Recall that 1997 had large positive loading on PC1 (typical El Niño) and large negative loading on PC2 (eastward shift of SST anomaly in Pacific), while 2002 had only modest positive loading on PC1 but strong loading on PC3. The reconstruction successfully captures the salient differences in rainfall for these two years. This includes the strong dry condition across most of southeastern Australia in 2002, and the less spatially coherent dry conditions in the northeast and southeast broken by wet conditions in the central east coast in 1997.

This reconstruction is also done for Australian-mean rainfall. Figure 11 shows the observed rainfall anomaly (hatched bar), and the reconstruction based on the first EOF (light-shaded bar), the first two EOFs (moderate-shaded bar), and the first three EOFs (dark-shaded bar) of SST. Recall that ~50% of the Australian-mean rainfall variance is accounted for by the first three EOFs of SST (Table 1). If only SST1 is taken into account in 1997, a large negative rainfall anomaly would have been expected. But, the large negative projection onto SST2 (Fig. 7d) substantially cancels much of the reduced rainfall predicted by SST1. In 2002, only a modest negative rainfall anomaly would have been expected based on the projection onto SST1. The strong positive projection onto SST3, however, predicts a stronger negative rainfall anomaly.

It is interesting to examine other years where projections onto the higher-order EOFs of SST play a significant role. For instance, strong dry conditions during the modest El Niño of 1994 are accounted for by positive projection onto SST2. This sensitivity also appears to carry over to some La Niña events. For instance, the very wet year of 1998 is accounted for by negative loading onto SST1 in conjunction with negative loading on SST2, which together yield a westward-shifted negative SST anomaly. Furthermore, the wet year of 1983 is accounted for by the negative projections onto SST2 and SST3 with minimal negative projection onto SST1. As might be expected due to internal noise, there are years, such as 1988, when the observed rainfall anomalies are not well accounted for by the linear relationship with the EOFs of SST. Overall, though, it appears that much of the inter–El Niño variability of Australian rainfall can be accounted for by the "flavor" of the individual El Niño events.

4. Reproducibility of sensitivity to central Pacific SST

To examine the robustness of the sensitivity of Australian rainfall to the detailed structure of tropical SST anomalies during El Niño, we reassess the observed relationship using independent data for an earlier period (1961–81). Numerical ensemble experiments with a BMRC general circulation model, forced by observed SST variations 1982–2002, have also been conducted to study Australian rainfall sensitivity to the details of SST forcing. The model results support our conclusions and will be reported elsewhere. In this section we focus on reproducibility of the sensitivity of Australian rainfall to SST using independent observations.

Different approaches can be used to assess the ro-

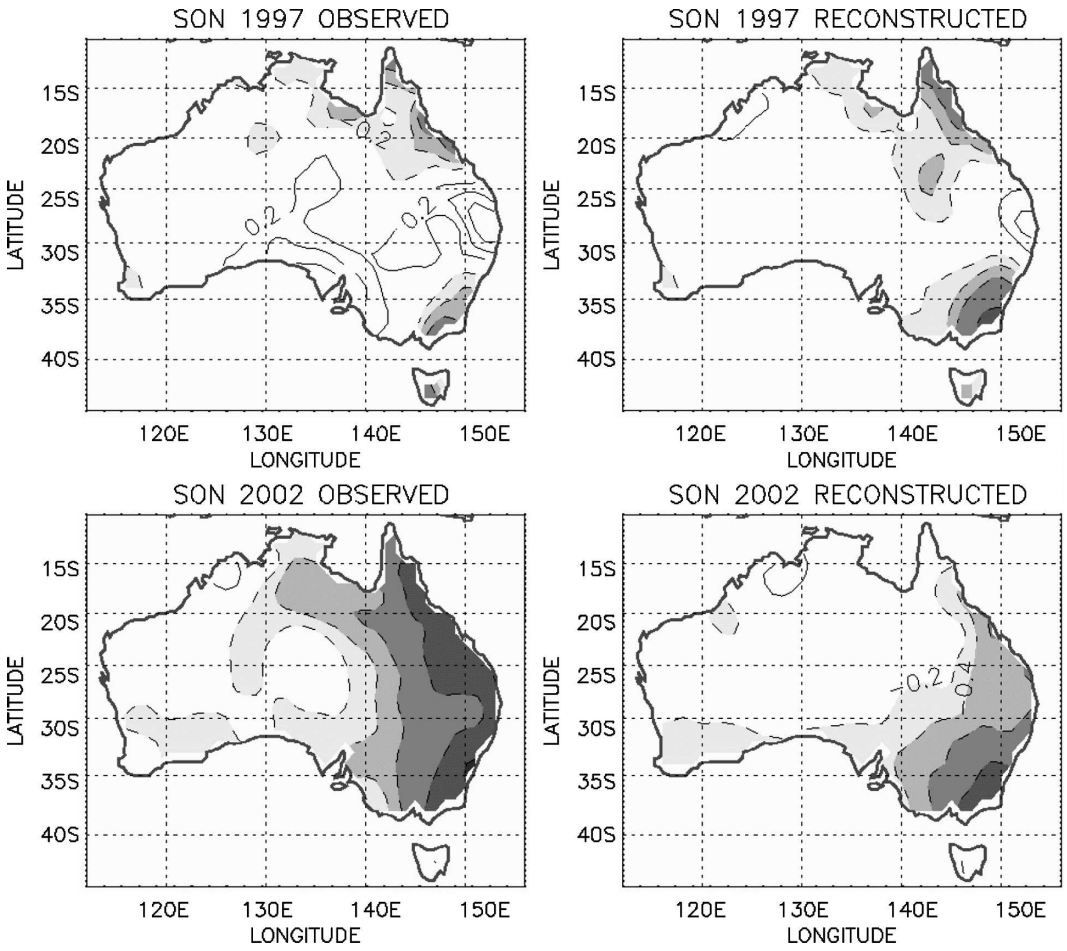

FIG. 10. Rainfall anomalies (left) observed and (right) reconstructed from regression onto the leading three EOFs of SST for SON (top) 1997 and (bottom) 2002. Positive and negative anomalies are drawn by solid and dashed lines, respectively. Negative rainfall also is highlighted with progressive shadings. Contour levels are at ± 0.2, 0.4, 0.6, 1 and 1.5 mm day^{-1}. Spatial smoothing has been applied before drawing.

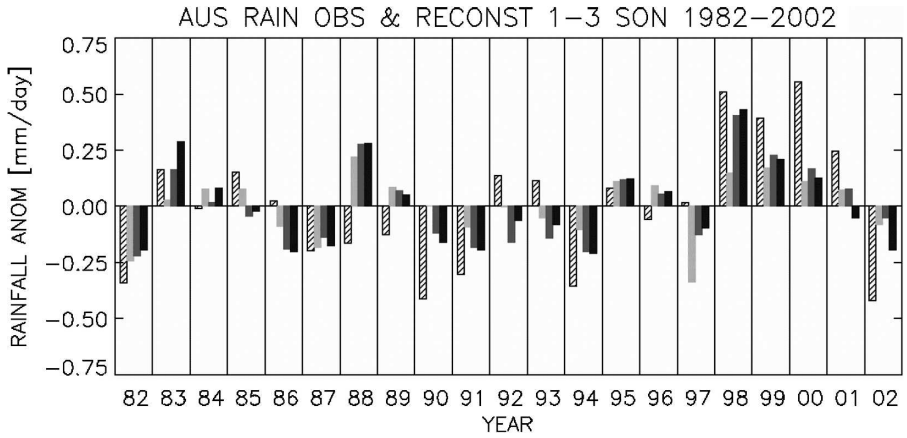

FIG. 11. Australian-mean rainfall anomalies for the SON season from observations (hatched bar), and from reconstruction based on SST EOF1 (light shading), EOFs 1 and 2 (moderate shading), and EOFs 1–3 (dark shading).

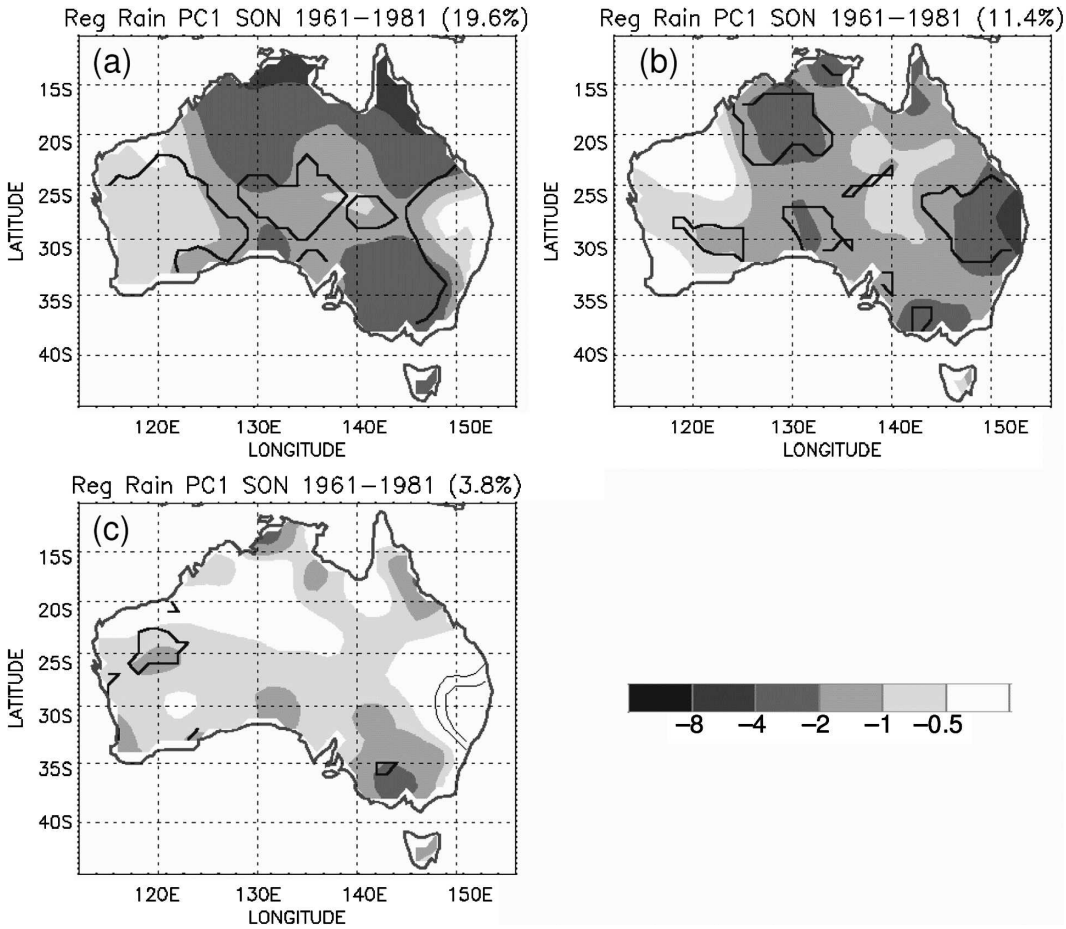

FIG. 12. Regression of Australian rainfall onto (a) SST1, (b) SST2, and (c) SST3 for the period SON 1961–81. Plotting convention is as in Fig. 9.

bustness of the observed sensitivity of Australian rainfall to the details of tropical Indo-Pacific SST variability. One option is to redo the EOF analysis of SST and correlation with rainfall using independent data from an earlier period. However, there is no guarantee that the derived EOFs of SST for the earlier period, especially the higher-order ones, will be recovered. Another approach is to project independent SST data from an earlier period onto the EOFs derived from the later period, and then investigate the relationship of the resulting PCs with rainfall for the earlier period. The advantage of this approach is that the sensitivity to the same SST patterns can be assessed, even though these SST patterns are not necessarily dominant, or at least not necessarily ranked in the same order. While sacrificing strict orthogonality of the projected PCs in the earlier period, we adopt the second approach.

Monthly mean SST analyses of Kaplan et al. (1998) for the period 1961–81 are used as independent data. They are projected onto the EOFs of SST derived for the later period (1982–2002). Whereas SST1 accounted for ~50% of the SST variance in the later period (Fig. 7a), it now accounts for ~40% of the variance in the earlier period. SST2 and SST3 account for less SST variance in the earlier period as well. However, the correlation of ADI with PC1, PC2, and PC3 for the earlier period is 0.62, 0.47, and 0.19, respectively. These correlations have the same sign and similar magnitude (correlations with PC1 and PC2 are actually stronger in the earlier record) as for the original PCs derived for the later period. These findings give us confidence that the sensitivity of Australian rainfall to the details of SST variations during El Niño is robust.

The spatial distribution of rainfall variability associated with the EOFs of SST is also retained in the earlier period. Figure 12 displays the regression patterns of gridded rainfall onto PCs 1–3 for the earlier period and should be compared to the equivalent patterns for the later period (Fig. 9). While some minor differences are evident for PCs 2 and 3 (e.g., wet signal in southeast for PC2 in the later period is replaced by dry signal in earlier period, and the dry signal on the central east

coast for PC3 in the later period is replaced by a wet signal in the earlier period), the overall agreement in pattern and magnitude is outstanding. Thus, negative loadings on SST2 or SST3 would still be inferred to mitigate drought conditions, especially in the southeast, predicted by positive loading on SST1.

5. Conclusions

Australia tends to experience drought during El Niño, but not all El Niños are equally influential. Drought usually develops during El Niño, especially in the eastern two-thirds of the continent during austral spring season, because the Walker circulation shifts eastward, resulting in higher surface pressure and anomalous sinking motion at Australian longitudes. El Niño events that develop with the strongest SST anomalies shifted into the far eastern Pacific (e.g., El Niño 1997) tend not to produce as severe a response as those events that are more focused near the date line (e.g., El Niño 2002). This sensitivity stems from the anomalous Walker circulation shifting too far east to effectively suppress Australian rainfall during El Niño events that maximize in the far eastern Pacific. While we have developed empirical evidence of a causal relationship between the anomalous zonal displacement of the Walker circulation and the strength of the Australian rainfall teleconnection, further work is required to elucidate the dynamical link.

This sensitivity to inter–El Niño variations of SST is hypothesized to be an explanation for the lack of a strong linear relationship between El Niño strength (as measured for instance by the Niño-3 SST index) and drought that was uncovered by Power et al. (2006). Drought depends not only on the SST anomaly magnitude encapsulated by the Niño-3 SST index but also on the west–east displacement of each El Niño event. Furthermore, the more robust linear relationship between La Niña strength and associated Australian rainfall increases reported by Power et al. (2006) may be similarly explained: The equatorial rainfall anomalies during La Niña tend to be shifted west of their oppositely signed anomalies during El Niño because tropical convection tends not to occur over SST below about 27°C (Hoerling et al. 1997). Hence, the Walker circulation anomaly during La Niña that favors enhanced Australian rainfall tends to be shifted west (i.e., closer to Australian longitudes) of the Walker circulation anomaly during El Niño that promotes drought.

The sensitivity of Australian rainfall, especially in the eastern two-thirds of the country in springtime, to the longitudinal structure of the SST during El Niño events suggests the possibility of additional predictability of Australian rainfall beyond that associated with just predicting the occurrence of El Niño. However, predictability of the inter–El Niño variations of SST has not been demonstrated. For instance, Drosdowsky and Chambers (2001) were not able to improve an empirical prediction scheme for Australian rainfall (based on observed lagged relationships between rainfall and EOFs of SST) by including additional EOFs of SST beyond the two leading modes in the Pacific and Indian Ocean basins. Nonetheless, dynamical prediction of the details of the SST anomalies during El Niño may be possible, if for instance, predictability stems from the details of the initial conditions that are unique to each event.

A similar sensitivity to the longitudinal distribution of SST anomalies during El Niño has also been recently demonstrated for the Indian summer monsoon (Kumar et al. 2006). El Niño events with the warmest SST anomalies in the central equatorial Pacific are more effective for driving a suppressed monsoon than are El Niño events with the warmest SST in the eastern equatorial Pacific. Although Kumar et al. focus on Indian monsoon rainfall during the northern summer season, they similarly conclude that the rainfall teleconnection during El Niño reflects the sensitivity of the Walker circulation to both the strength and the location of SST anomalies.

Finally, we have focused on inter–El Niño variations of the longitudinal distribution of SST anomaly as the cause of inter–El Niño variations of the impact in Australia. However, additional mechanisms cannot be dismissed as drivers of interannual variations in seasonal rainfall variability. For instance, land surface conditions may have contributed to the different responses in 1997 and 2002. Rainfall in autumn (March–May) and winter (June–August) were near normal in 1997 but already dry in 2002. Thus, land surface conditions were already dry leading into spring 2002, which would then presumably amplify drought promoted by the positive SST anomalies near the date line. Additional climate model experiments using a range of land surface initializations might quantify this effect.

Acknowledgments. We thank S. Power, S. Grainger, and the anonymous reviewers for constructive comments on earlier versions of the manuscript. Support for this research was provided, in part, by the South East Australian Climate Initiative.

REFERENCES

Allan, R. J., 1988: El Niño southern oscillation influences in the Australian region. *Prog. Phys. Geogr.,* **12,** 313–348.

Drosdowsky, W., and L. E. Chambers, 2001: Near-global sea sur-

face temperature anomalies as predictors of Australian seasonal rainfall. *J. Climate,* **14,** 1677–1687.

Gill, A. E., 1980: Some simple solutions for heat-induced tropical circulation. *Quart. J. Roy. Meteor. Soc.,* **106,** 447–462.

Goddard, L., S. J. Mason, N. E. Graham, and W. Thiaw, 1998: Climate surprises of the 1997–1998 El Niño. *Proc. 23d Annual Climate Diagnostics and Prediction Workshop,* Miami, FL, NOAA, 34–37.

——, ——, S. E. Zebiak, C. F. Ropelewski, R. Basher, and M. A. Cane, 2001: Current approaches to seasonal to interannual climate predictions. *Int. J. Climatol.,* **21,** 1111–1152.

Graham, N. E., and T. P. Barnett, 1987: Sea surface temperature, surface wind divergence and convection over tropical oceans. *Science,* **238,** 657–659.

Hoerling, M. P., and A. Kumar, 2002: Atmospheric response patterns associated with tropical forcing. *J. Climate,* **15,** 2184–2203.

——, ——, and M. Zhong, 1997: El Niño, La Niña, and the nonlinearity of their teleconnections. *J. Climate,* **10,** 1769–1786.

Jones, D. A., and G. Weymouth, 1997: An Australian monthly rainfall dataset. Tech. Rep. 70, Bureau of Meteorology, Melbourne, Australia, 19 pp.

Kanamitsu, M., W. Ebisuzaki, J. Woollen, S.-K. Yang, J. J. Hnilo, M. Fiorino, and G. L. Potter, 2002: NCEP–DOE AMIP-II reanalysis (R-2). *Bull. Amer. Meteor. Soc.,* **83,** 1631–1643.

Kaplan, A., M. Cane, Y. Kushnir, A. Clement, M. Blumenthal, and B. Rajagopalan, 1998: Analyses of global sea surface temperature 1856–1991. *J. Geophys. Res.,* **103,** 567–589.

Kumar, A., and M. P. Hoerling, 1997: Interpretation and implications of the observed inter–El Niño variability. *J. Climate,* **10,** 83–91.

Kumar, K., B. Rajagopalan, M. Hoerling, G. Bates, and M. Cane, 2006: Unraveling the mystery of Indian monsoon failure during El Niño. *Science,* **314,** 115–119.

Liebmann, B., and C. A. Smith, 1996: Description of a complete (interpolated) outgoing longwave radiation dataset. *Bull. Amer. Meteor. Soc.,* **77,** 1275–1277.

Lu, L., and D. Hedley, 2004: The impact of the 2002–03 drought on the economy and agricultural employment. Economic Roundup Autumn 2004, The Treasury, Australian Government, 25–44. [Available online at http://www.treasury.gov.au/documents/817/PDF/roundup_autumn_2004.pdf.]

McBride, J. L., and N. Nicholls, 1983: Seasonal relationships between Australian rainfall and the Southern Oscillation. *Mon. Wea. Rev.,* **111,** 1998–2004.

Nicholls, N., 1989: Sea surface temperatures and Australian winter rainfall. *J. Climate,* **2,** 965–973.

Potgieter, A. B., G. L. Hammer, H. Meinke, R. C. Stone, and L. Goddard, 2005: Three putative types of El Niño revealed by spatial variability in impact on Australian wheat yield. *J. Climate,* **18,** 1566–1574.

Power, S., M. Haylock, R. Colman, and X. Wang, 2006: The predictability of interdecadal changes in ENSO activity and ENSO teleconnections. *J. Climate,* **19,** 4755–4771.

Rasmusson, E., and T. Carpenter, 1982: Variations in the tropical sea surface temperature and surface wind fields associated with the Southern Oscillation/El Niño. *Mon. Wea. Rev.,* **110,** 354–384.

Reynolds, R. W., and T. M. Smith, 1994: Improved global sea surface temperature analysis using optimum interpolation. *J. Climate,* **7,** 929–948.

Ropelewski, C. F., and M. S. Halpert, 1987: Global and regional scale precipitation patterns associated with El Niño/Southern Oscillation. *Mon. Wea. Rev.,* **115,** 1606–1626.

Sardeshmukh, P. D., and B. J. Hoskins, 1988: The generation of global rotational flow by steady idealized tropical divergence. *J. Atmos. Sci.,* **45,** 1228–1251.

Trenberth, K. E., and D. P. Stepaniak, 2001: Indices of El Niño evolution. *J. Climate,* **14,** 1697–1701.

——, G. W. Branstator, D. Karoly, A. Kumar, N.-C. Lau, and C. Ropelewski, 1998: Progress during TOGA in understanding and modeling global teleconnections associated with tropical sea surface temperatures. *J. Geophys. Res.,* **103,** 291–324.